Author's personal copy

Applied Catalysis A: General 427–428 (2012) 98–105

Contents lists available at SciVerse ScienceDirect

Applied Catalysis A: General

journal homepage: www.elsevier.com/locate/apcata

Transformations of monoterpene hydrocarbons on ferrierite type zeolites

R. Rachwalik[a], M. Hunger[b], B. Sulikowski[c,*]

[a] Institute of Organic Chemistry and Technology, Faculty of Engineering and Chemical Technology, Cracow University of Technology, Warszawska 24, 31-155 Kraków, Poland
[b] Institute of Chemical Technology, University of Stuttgart, 70550 Stuttgart, Germany
[c] Jerzy Haber Institute of Catalysis and Surface Chemistry, Polish Academy of Sciences, Niezapominajek 8, 30-239 Kraków, Poland

ARTICLE INFO

Article history:
Received 8 December 2011
Received in revised form 22 February 2012
Accepted 27 March 2012
Available online 3 April 2012

Keywords:
Ferrierite
Isomerization
α-Pinene
Limonene
Camphene
Secondary reactions

ABSTRACT

Transformations of α-pinene and limonene over hydrogen forms of commercial ferrierite type zeolites of different origin (Tosoh Corp. and Zeolyst Intern.) have been studied in the liquid phase at 313–363 K. The catalysts were characterized by XRD, sorption of nitrogen, scanning electron microscopy, FTIR and ^{27}Al & ^{1}H MAS NMR. The concentration of Brønsted acid sites has been determined by ^{1}H MAS NMR and FTIR quantitative measurements, while their strength was estimated by adsorption of CO. The liquid-phase isomerization of α-pinene proceeds smoothly on the two zeolite catalysts, and the initial reaction rates have been compared. Camphene and limonene were the main products, while the selectivity to these hydrocarbons differed. Isomerization of pure limonene was also studied, showing large difference in activity over the two ferrierite catalysts. The selectivity of α-pinene transformations has been rationalized in terms of retarded consecutive isomerization of limonene over the zeolite from Zeolyst.

© 2012 Elsevier B.V. All rights reserved.

1. Introduction

Monoterpenes constitute a sub-group of terpenes, various compounds occurring in nature as components of essential oils (mainly in plants). They consist of two isoprene units (2-methyl-1,3-butadiene, corresponding to $C_{10}H_{16}$) and can be classified into three main arbitrary categories: acyclic, monocyclic and bicyclic [1]. Monoterpenes are particularly interesting from a fine chemical synthesis standpoint. The chief sources of the monoterpenes and their derivatives are the essential oils obtained by distillation or extraction under pressure of various plant parts: flowers, leaves, roots, rhizome, wood, bark, fruit and seeds [2,3]. The major industrial source of monoterpene hydrocarbons is crude sulphate turpentine obtained from wood pulp as a waste product in the manufacture of cellulose via the sulphate process. A minor source of bicyclic terpene hydrocarbons is wood turpentine that is obtained by the steam distillation of chopped tree trunks and dead wood. The crude sulphate turpentine is a complex mixture of C_{10} hydrocarbons composed mostly of α-pinene (60–65%), β-pinene (25–35%) and other monocyclic terpenes, such as limonene. α-Pinene and β-pinene are distilled off from the crude sulphate turpentine and used to produce a variety of flavour and fragrance materials [1,2]. Transformation of α-pinene over solid acids by two routes yields: (i) bicyclic products of the camphene series; and (ii) monocyclic products like limonene, *p*-cymene and other (cf. Scheme 1) [4,5].

Isomerization of α-pinene is of industrial significance because camphene is an intermediate compound for commercial chemicals, such as synthetic camphor, toxaphene and isobornyl acetate. Camphor is applied, inter alia, as a counterirritant, anaesthetic, expectorant, and antipruritic agent. It is also used as a substrate in manufacturing terpene phenolic resins, as a plasticizer for paints, resins and also in the synthesis of acrylates and methacrylates [6,7].

Generally, the main method for manufacture of camphene is based on the isomerization of α-pinene in the presence of a weakly acidic TiO_2 catalyst in the hydrated state (titania modified by sulphuric acid). The process is carried out in the liquid phase using stirred tank reactors at 403–418 K [8,9], resulting in considerable waste streams and corrosion problems. Therefore, all works concern to design highly active and selective solid acid catalysts suitable for the replacement of the currently applied material. Solid catalysts offer several advantages: facility of the easy catalysts separation from the reaction mixture makes neutralization superfluous, while corrosion is minimized, and the catalysts can be applied several times. Isomerization of α-pinene has been tested over various acidic catalysts: modified zeolites [10–16], oxides treated with acids [17–19], activated clays [20,21] and heteropoly-acids [22–24].

The aim of this work was to study catalytic transformations of monoterpene hydrocarbons, α-pinene and limonene, over two ferrierite type zeolites of different origin. The samples were obtained from Tosoh Corp. and Zeolyst Intern. companies, respectively. All

* Corresponding author. Tel.: +48 12 6395 159; fax: +48 12 425 1923.
E-mail address: ncsuliko@cyf-kr.edu.pl (B. Sulikowski).

0926-860X/$ – see front matter © 2012 Elsevier B.V. All rights reserved.
http://dx.doi.org/10.1016/j.apcata.2012.03.037

Author's personal copy

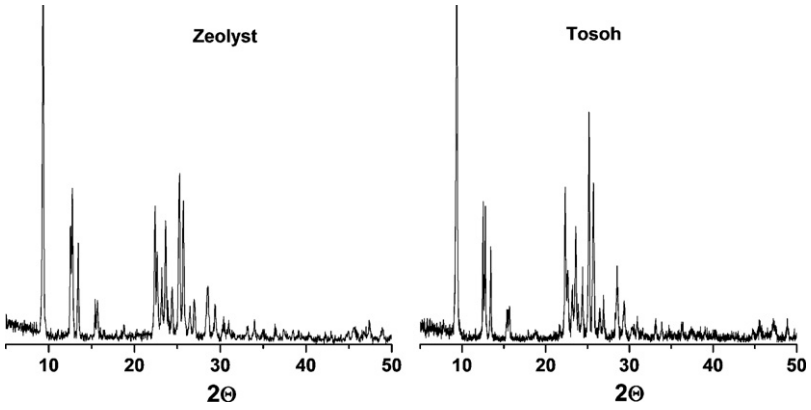


Fig. 1. X-ray diffraction patterns of the hydrated hydrogen forms of ferrierite from Zeolyst and Tosoh.

the catalytic tests were carried out using a batch reactor working at 313–363 K. The samples were characterized quantitatively by ^{1}H MAS NMR and FTIR spectroscopies. In particular, FTIR spectroscopy was used for estimating the strength of Brønsted acid sites.

2. Experimental

2.1. Preparation of samples

The two commercial ferrierite type zeolites, K,Na-FER (Si/Al = 8.9) and NH_4-FER (Si/Al = 10.0), were obtained from Tosoh Corporation (Japan) and Zeolyst International (US), respectively. The ammonium form of the ferrierite from Tosoh was obtained by an ion-exchange of a zeolite K,Na-FER with an 0.5 M aqueous solution of ammonium nitrate. The ion-exchange process was repeated four times at room temperature for 12 h each. The ammonium-exchanged sample was washed with doubly distilled water and dried at 373 K overnight. Finally, the ammonium forms of ferrierite were calcined in air at 773 K for 5 h to yield the hydrogen forms, labelled H-FER (T) or (Z).

2.2. Adsorption properties

Adsorption of nitrogen was carried out using the Quantachrome Autosorb Automated Gas Sorption System. Prior to the measurements, the samples were outgassed at 473 K for 24 h.

2.3. SEM microscopy

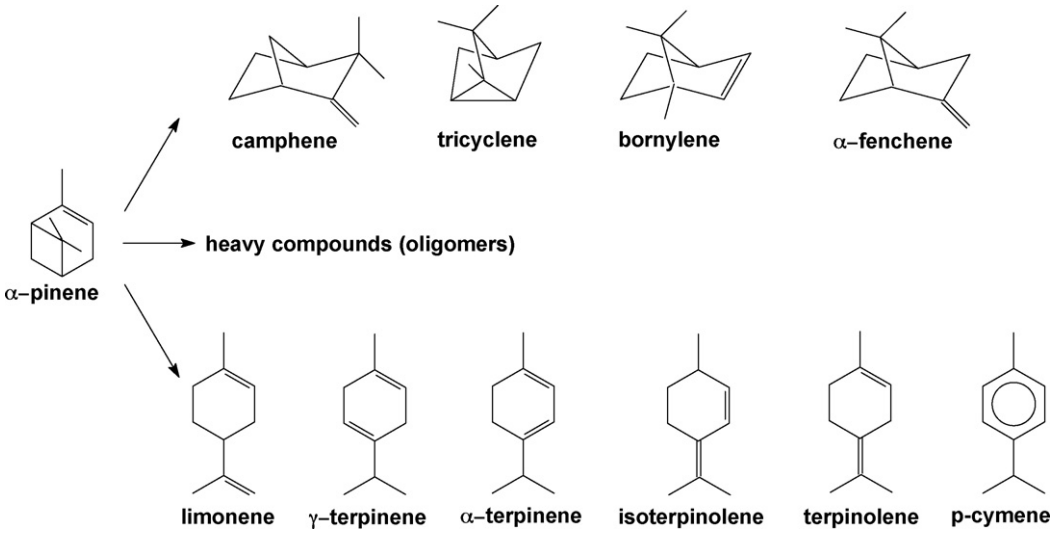
The SEM pictures were taken with a Philips XL30 instrument.

2.4. MAS NMR spectroscopy

The ^{27}Al MAS NMR spectra were acquired using a Bruker Avance III 500 MHz spectrometer working at a magnetic field of 11.7 T, with short 0.3 μs single-pulse excitations ($\pi/10$), a repetition time of 0.5 s and 6144 accumulations. The fully hydrated samples were spun at 14 kHz in 4-mm zirconia rotors. The ^{1}H MAS NMR spectra were measured using a Bruker MSL400 spectrometer at a magnetic field of 9.4 T, with single-pulse excitations of 2.2 μs ($\pi/2$), the repetition time of 30 s, 160 accumulations, and a sample spinning rate of ca. 8 kHz. Prior to the ^{1}H MAS NMR studies, the samples were dehydrated at 723 K for 12 h in a vacuum of $p < 10^{-6}$ bar. The ^{1}H MAS NMR intensities were evaluated taking into account the accumulation numbers and the sample weights. The concentration of Brønsted protons was determined by comparing the signal integrals with that of a reference material.

2.5. FTIR spectroscopy

FTIR studies of CO adsorption at temperature of liquid nitrogen were performed on self-supported discs of zeolites (ca. 10 mg/cm^2) on a Bruker 48 PC spectrometer equipped with an MCT detector



Scheme 1.

Author's personal copy

at a spectral resolution of 2 cm^{-1}. In most cases, 100–200 scans were accumulated. The ferrierite samples were activated in situ in the IR cell at 803 K for 2 h under a vacuum of $p < 10^{-6}$ Pa. All FTIR spectra shown in this work were normalized taking into account the sample weights. The amount of Brønsted acid sites (i.e., the bridging Si—O(H)—Al groups) was estimated by NH_3 adsorption, while their strength was calculated from shift of the O—H bond stretching vibrations upon adsorption of CO [30].

2.6. Catalytic tests

The ferrierite samples were tested in the isomerization of α-pinene and limonene. Isomerization was carried out at atmospheric pressure in a glass reactor equipped with a reflux condenser, an efficient stirrer (~800 r.p.m.) and a temperature controller. In a typical run, 5 ml of α-pinene or limonene (both from Aldrich) was heated to desired reaction temperature. Before addition to the reaction mixture, the catalyst (0.25 g) was calcined at 673 K for 5 h in a helium flow. The catalytic tests were carried out at the 313–363 K and 313–348 K temperature range for α-pinene and limonene transformations, respectively. After selected times, 10-μL aliquots of the reaction mixture were obtained for gas chromatography (GC) analysis.

Conversion and selectivity were calculated as shown below:

$$\text{conversion of } \alpha\text{-pinene} = \left[\frac{c^0_{\alpha\text{-pinene}} - c_{\alpha\text{-pinene}}}{c^0_{\alpha\text{-pinene}}}\right] \cdot 100\%$$

$$\text{selectivity to camphene} = \left[\frac{c_{\text{camphene}} - c^0_{\text{camphene}}}{c^0_{\alpha\text{-pinene}} - c_{\alpha\text{-pinene}}}\right] \cdot 100\%$$

$$\text{selectivity to limonene} = \left[\frac{c_{\text{limonene}}}{c^0_{\alpha\text{-pinene}} - c_{\alpha\text{-pinene}}}\right] \cdot 100\%,$$

where $c_{\alpha\text{-pinene}}$, c_{camphene}, and c_{limonene} denote the concentration (mol%) of α-pinene, camphene and limonene in the reaction products, respectively. The initial concentrations of α-pinene and camphene are labelled $c^0_{\alpha\text{-pinene}}$ and c^0_{camphene}. The concentrations of α-pinene and camphene in the feed were 98.63 and 1.13 mol%, respectively. The conversion to limonene was calculated:

$$\text{conversion of limonene} = \left[\frac{c^0_{\text{limonene2}} - c_{\text{limonene2}}}{c^0_{\text{limonene2}}}\right] \cdot 100\%,$$

where $c^0_{\text{limonene2}}$ and $c_{\text{limonene2}}$ are the concentrations (mol%) of limonene in the feed and in the limonene isomerization products, respectively.

3. Results and discussion

X-ray diffraction patterns of the two commercial samples revealed characteristic diffraction lines consistent with the structure of ferrierite (FER) and good crystallinity. Ion exchange of ferrierite from Tosoh with ammonium nitrate solution did not affect the X-ray pattern. Similarly, calcination of the two ammonium forms to yield the corresponding hydrogen forms did not result in any significant change in XRD (Fig. 1). Crystallinity of the hydrogen forms, estimated on the basis of XRD patterns, was high (>95%). The specific surface areas of the samples were very close (287 and 275 m^2/g), and the H-FER (T) sample had slightly lower Si/Al ratio (Table 1).

The SEM microphotographs of the two zeolites from Zeolyst (Fig. 2a and c) and Tosoh (Fig. 2b and d) show nearly spherical agglomerates uneven in size composed of smaller plate-like crystals. The agglomerates are larger and more uniform in size in the case of the sample from Tosoh. The plate-like crystals are in the range of 300–500 nm.

The main information, which can be obtained by ^{27}Al MAS NMR spectroscopy, is the distribution of aluminium atoms between framework and non-framework positions. In the ^{27}Al MAS NMR spectra (Fig. 3a and b) the strong signals at 55 ppm are attributed to tetrahedrally coordinated framework aluminium atoms. Additionally, in both spectra the second weak signals at 0 ppm could be discerned, indicating the presence of octahedrally coordinated extra-framework aluminium species. The intensities of these signals were equal to 15.6% for H-FER (Z) and 6.1% for H-FER (T), respectively. Thus, ca. 2.5 times more octahedral aluminium was present in the sample from Zeolyst (Fig. 3a).

^{1}H MAS NMR spectroscopy was used for quantitative and qualitative assessment of different kinds of proton sites and the concentration of Brønsted acid sites in the ferrierite samples, respectively. The proton spectra differ significantly, and the main difference is, in addition to the bridging hydroxyl groups Si—O(H)—Al at 4.2 ppm (i.e., the Brønsted acid sites [25]), the presence of relatively strong signals at 1.8 and 2.8 ppm in the spectrum of H-FER (Z) (Fig. 4a). The isolated silanols groups at 1.8 ppm in this sample are abundant, possibly due to smaller and/or more defected ferrierite crystals from Zeolyst. In the spectrum of H-FER (T), the signal of Brønsted acid sites at 4.2 ppm essentially dominates, while the signal of silanol groups at 1.8 ppm is weak (Fig. 4b). The strong signal at 2.8 ppm in H-FER (Z) was assigned to the presence of hydroxyl groups bounded to *extraframework* aluminium species (AlOH) [26]. It is a direct evidence that a part of the aluminium atoms exists as non-framework species, not inserted into the T framework positions during hydrothermal synthesis and located in the pore system and at the surface of crystals. The intensity of this ^{1}H MAS NMR signal agrees very well with the ^{27}Al MAS NMR signal at ca. 0 ppm, showing the ca. 16% of the aluminium atoms are located outside the aluminosilicate framework (Fig. 3a and Table 1). Finally, a weak ^{1}H MAS NMR signal at ca. 6 ppm is assigned to hydroxyl protons interacting with the extraframework aluminium species via hydrogen bonding [27]. The intensity of this signal is higher in the spectrum of zeolite H-FER (Z), in accord with what was considered above.

A signal of protons at 4.2 ppm was used in this work to calculate the concentration of Brønsted acid sites in the ferrierite samples, and the results are given in Table 1. As seen, the concentration of Brønsted acid sites in the sample H-FER (T) is higher in comparison to the other material. Moreover, the concentration of acid sites in the second sample is much lower than the amount of tetrahedrally coordinated aluminium atoms, connected via oxygens with these hydroxyl protons. The negative framework charges must be, therefore, compensated, at least in part, by extraframework aluminium species contributing also to the ^{1}H MAS NMR signal at 2.8 ppm. Such a picture was also confirmed by IR spectroscopy (vide infra).

The IR spectrum of the H-FER (T) zeolite consists of three main bands at 3748, 3600 and 3550 cm^{-1} (Fig. 5). These bands were assigned to: (i) the external, terminal silanol groups Si—OH and (ii) the bridging Si—O(H)—Al groups located inside the 10-ring channels and inside the ferrierite cages, respectively. Additionally, a small hump at 3650 cm^{-1} can be discerned in the spectrum due to *extraframework* AlOH species [28].

The H-FER (Z) zeolite exhibits essentially a similar FTIR spectrum, however, some differences can be noticed. First, the main band corresponding to Brønsted acid sites at 3600 cm^{-1} is broader. Second, the hump at the 3650 cm^{-1} is more pronounced, in line with the ^{27}Al and ^{1}H MAS NMR signals of extraframework AlOH groups. And third, there are less external silanol groups at 3748 cm^{-1}, while an additional hump at ca. 3730 cm^{-1} can

Author's personal copy

Table 1
Characteristics of the two hydrogen forms of ferrierite.

Samples	Si/Al[a]	SSA[b] [m^2/g]	Concentration of Brønsted acid sites [mmol/g]			Strength of acid sites[d]	
			^{1}H MAS NMR[c]	FTIR[d]	av.	$\Delta\nu_{CO}$ [cm^{-1}]	PA[e] [kJ/mol]
H-FER (Z)	10.0	287	0.904	0.840	0.872	295	1162
H-FER (T)	8.9	275	1.389	1.172	1.281	286	1168

[a] Determined by chemical wet analysis.
[b] SSA – specific surface area.
[c] Determined by ^{1}H MAS NMR spectroscopy.
[d] Determined by ammonia adsorption using FTIR spectroscopy.
[e] The Proton Affinity calculated according to an equation in Ref. [30].

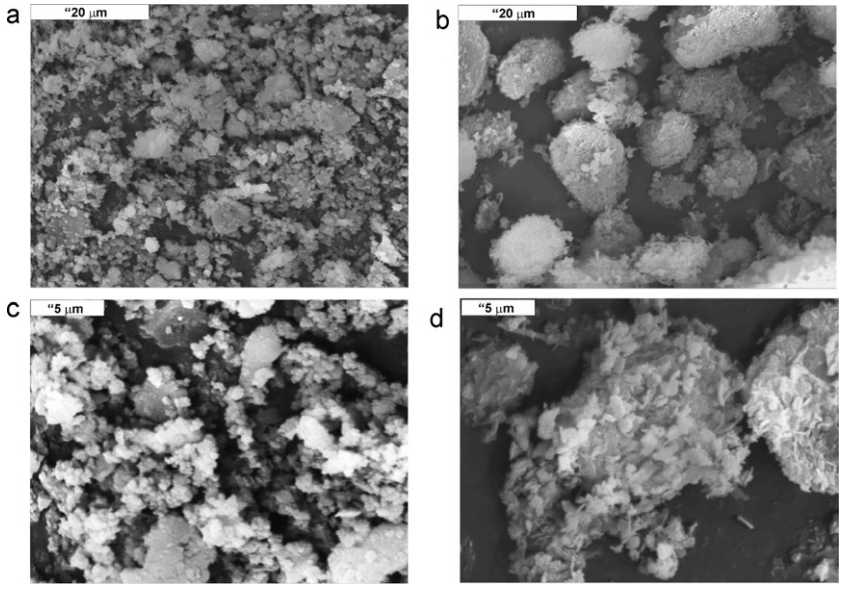


Fig. 2. SEM microphotographs of ferrierite samples: (a, c) H-FER (Z); (b, d) H-FER (T).

be discerned. The latter signal can be assigned to the internal silanol groups located inside the zeolitic faults, thus confirming that ferrierite from Zeolyst contains more faults. Finally, a broad shoulder at 3450–3550 cm^{-1} can be related to the hydrogen-bonded Si—O(H)—Al groupings [29]. All these observations are in line with the results of ^{27}Al and ^{1}H MAS NMR spectroscopy discussed above.

The strength of Brønsted acid sites was estimated by comparing the shift $\Delta\nu_{CO}$ (cm^{-1}) of the OH stretching vibrations

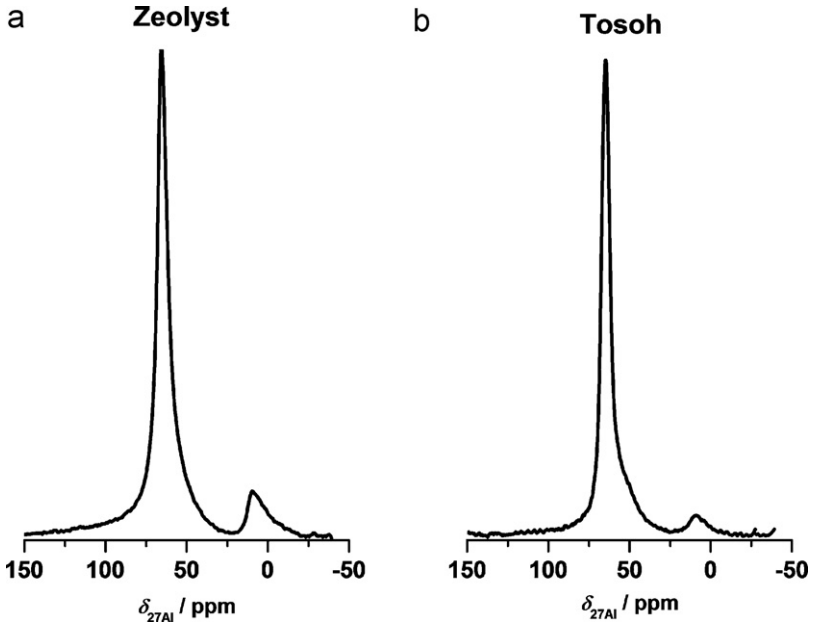


Fig. 3. ^{27}Al MAS NMR spectra of the hydrated samples: (a) H-FER (Z); (b) H-FER (T). The spectra were acquired using a Bruker 500 MHz spectrometer (11.7 T) with 0.3 μs single-pulse excitations (π/10), the repetition time of 0.5 s and 6144 accumulations.

Author's personal copy

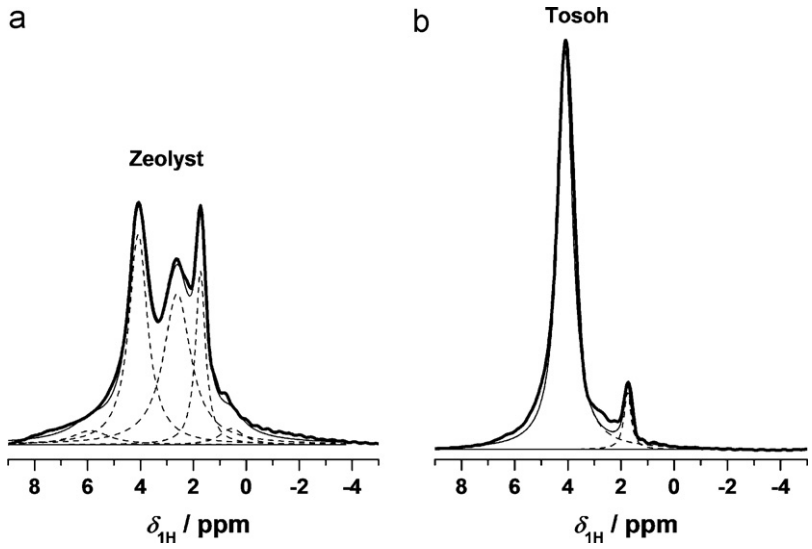


Fig. 4. ^{1}H MAS NMR spectra of dehydrated samples: (a) H-FER (Z); (b) H-FER (T). The ^{1}H MAS NMR spectra were measured using a Bruker MSL400 spectrometer (9.4 T) with 2.2 μs single-pulse excitations ($\pi/2$), the repetition time of 30 s and 160 accumulations.

after adsorption of CO. The corresponding values are 295 cm^{-1} and 286 cm^{-1} for the Zeolyst and Tosoh samples (Table 1). The adsorbate-induced band shift $\Delta\nu_{CO}$ can be related to the proton affinity of the Brønsted acid sites. A relationship between the observed band shift $\Delta\nu_{CO}$ (cm^{-1}) and the proton affinity (PA, kJ/mol) can be calculated according to a formula given in Ref. [30]: PA = 2254.8–442.5 log($\Delta\nu$). Hence, the calculated proton affinities of the two H-FER samples are 1162 and 1168 kJ/mol (Table 1). These data can be conveniently compared with that found for mordenite (1231 kJ/mol for hydroxyl protons located in side pockets, and 1158 kJ/mol for those located in the main channels), zeolite beta (1156 kJ/mol) and non-acidic hydroxyl protons on SiO_2 (1451 kJ/mol) [29,32]. It becomes clear that the Brønsted acid sites of the two ferrierites are comparable to the acid sites located in the main channels of mordenite and zeolite beta, but they are slightly weaker in their acid strength. Finally, the overall concentration of Brønsted acid sites in the H-FER (Z) sample is lower and the acid sites exhibit a higher strength (Table 1). The higher strength of the acid sites in H-FER (Z) can be rationalized taking into account two points: a slightly higher Si/Al ratio in this sample and the presence of more *extraframework* aluminium species (16%), as documented by solid-state NMR and FTIR spectroscopy. The interaction of the extraframework aluminium species with the Brønsted acid sites increases their acid strength. Such a situation is frequently encountered in weakly dealuminated zeolites.

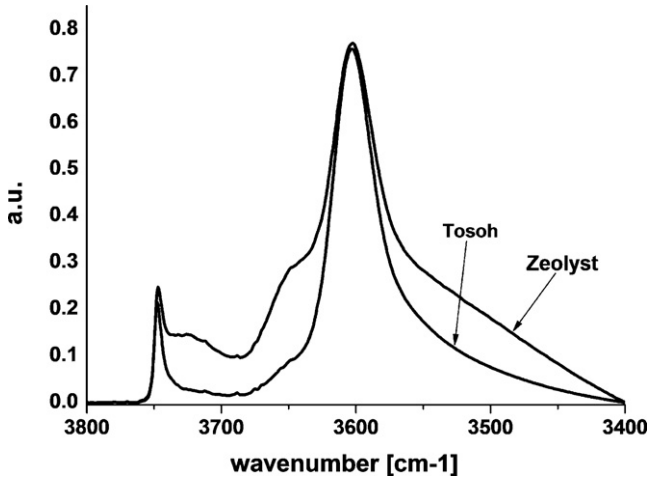


Fig. 5. FTIR spectra of two dehydrated hydrogen forms of ferrierite: (a) H-FER (Z); (b) H-FER (T).

The transformation of α-pinene over the two hydrogen forms of ferrierite of different origin was studied in the liquid phase. The main products are camphene and limonene, accompanied by smaller amounts of α- and γ-terpinene, terpinolene and *p*-cymene. The conversion levels over the catalysts are compared in Fig. 6. As seen, at the beginning the α-pinene conversion over the ferrierite catalysts increases rapidly and then levels out. It is also characteristic, and found for other zeolites [15,16], that the maximum conversion levels are not corresponding to the highest temperature studied (363 K). In our studies the highest conversion of α-pinene was observed at 348 K for H-FER (Z) and 338–348 K for H-FER (T). This point will be discussed further below.

The initial rate of α-pinene transformation was compared in Table 2, taking into account the average amount of Brønsted acid sites in the catalysts, as quantified by ammonia adsorption and ^{1}H MAS NMR studies. We note that according to our earlier findings, α-pinene is adsorbed in the ferrierite channel system and interacts with the acid sites located there, as its molecular dimensions (6.77 × 6.91 Å) are comparable with that of benzene [14,16]. The initial reaction rate over H-FER (Z) at 313 and 338 K is considerably lower, but increases sharply at higher temperatures approaching 8.8 mmol/mmol H^+ min (Table 2). On the other hand, the initial reaction rate over H-FER (T), higher at the beginning, equals to the other catalyst at 348 K and then decreases. We note that the initial reaction rates on the two ferrierite catalysts are generally higher than those observed for other catalysts, exemplified by heteropolyacids supported on silica and sulphonated zirconium dioxide [14].

Table 2
Initial rates of α-pinene transformations over ferrierite catalysts, normalized to the (average) amount of Brønsted acid sites.

Temperature (K)	Initial reaction rate of α-pinene [mmol/1 mmol H^+ min]	
	H-FER (Z)	H-FER (T)
313	1.97	2.87
338	1.83	4.96
348	4.99	4.97
363	8.78	3.29

Author's personal copy

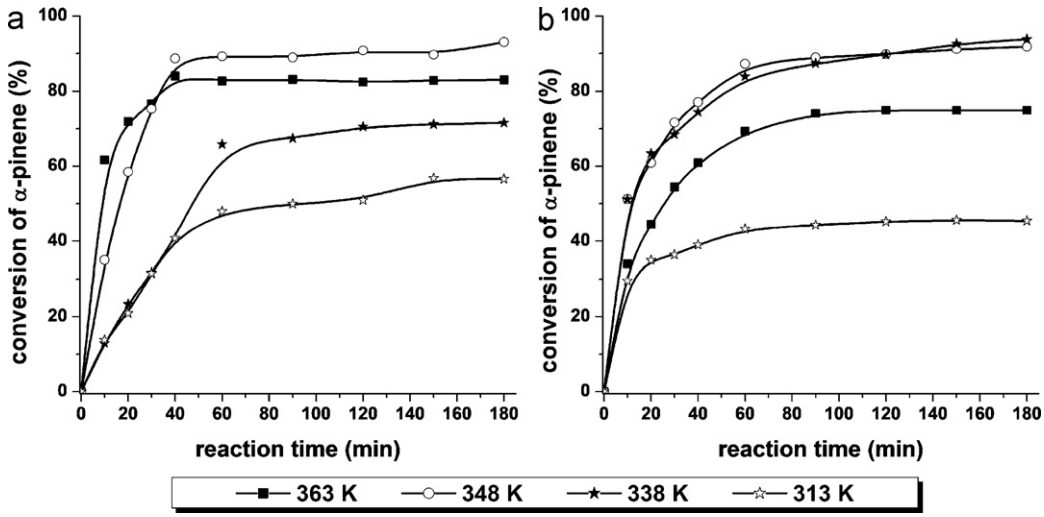


Fig. 6. Conversion of α-pinene at 313–363 K vs. the reaction time on: (a) H-FER (Z); (b) H-FER (T). The amount of a catalyst precalcined at 673 K: 0.25 g. Substrate: 5 ml of α-pinene.

The highest conversion was observed at lower reaction temperatures, i.e. 338–348 K (Fig. 6a and b). Further increasing the reaction temperature leads to *lower* overall activity. Such behaviour can be explained by considering the lower deactivation of zeolite materials at 348 K. During transformations of terpene hydrocarbons, some by-products are formed. It is evident that at higher temperature (363 K), in addition to isomerization products, formation of high-retention-time-products (HRTP) is more pronounced. The precise nature of the HRTP products is not yet known. Among them are oligomeric products containing multiple chemical bonds. The HRTP products might consist of dimers, trimers and higher oligomers. Specifically, dimers constitute the main part of reaction products when β-pinene is reacted over montmorillonite functionalized with sulphonic groups and perfluorinated sulphonic acid resin (Nafion) [31]. Formation of oligomeric species is visible by observing the catalyst colour, by GC and IR measurements (characteristic bands of C—H and C—C bonds). Oligomers constitute 'coke' precursors, similar to those appearing on zeolite catalysts working in the gas phase reactions. They can block effectively the access of substrate to the zeolite channels and acid sites located there. The amount of HRTP at 348 K was 3.3 and 10.1% for ZSM-5 and ZSM-12, and increased considerably to 6.7 and 14.9%, respectively, upon increasing the reaction temperature to 363 K [16]. A pronounced formation of HRTP over ferrierite manifests itself in decreasing the conversion of α-pinene at 363 K.

Camphene and limonene are the main hydrocarbons formed by α-pinene transformation. The highest total selectivity to these products is ca. 90%. The selectivity to camphene increases with temperature and is essentially steady with the reaction time (Fig. 7). A systematically higher selectivity to camphene is observed over the H-FER (T) sample. The high selectivity to this monoterpene can be attributed to its high stability. Once formed, it is not transformed easily by consecutive reactions, especially if one takes into account the lower strength of Brønsted acid sites in this catalyst.

The second valuable product formed by α-pinene isomerization is limonene, and the selectivity to this hydrocarbon vs. time is visualized in Fig. 8. The selectivity at 363 K is constant with the reaction time, equal to 45 and 35% on the two catalysts. At temperatures of 338–348 K, the selectivity over H-FER (T) clearly drops down with time (about 10%). The decrease of selectivity to limonene on

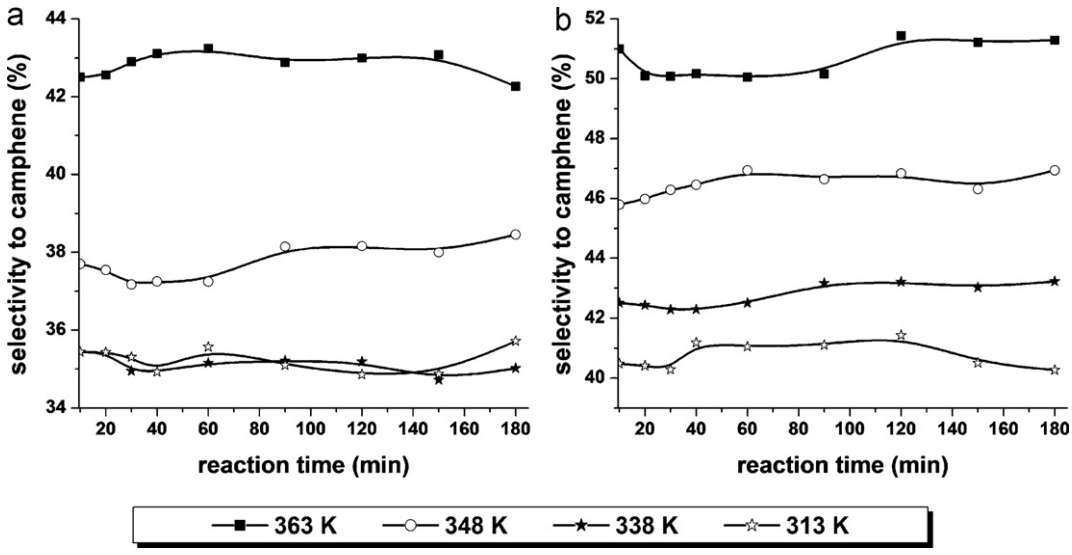


Fig. 7. Selectivity towards camphene as a function of the reaction time for the isomerization of α-pinene over H-ferrierite from Zeolyst (a) and Tosoh (b) at 313–363 K. The conditions of catalytic tests were as in Fig. 6.

Author's personal copy

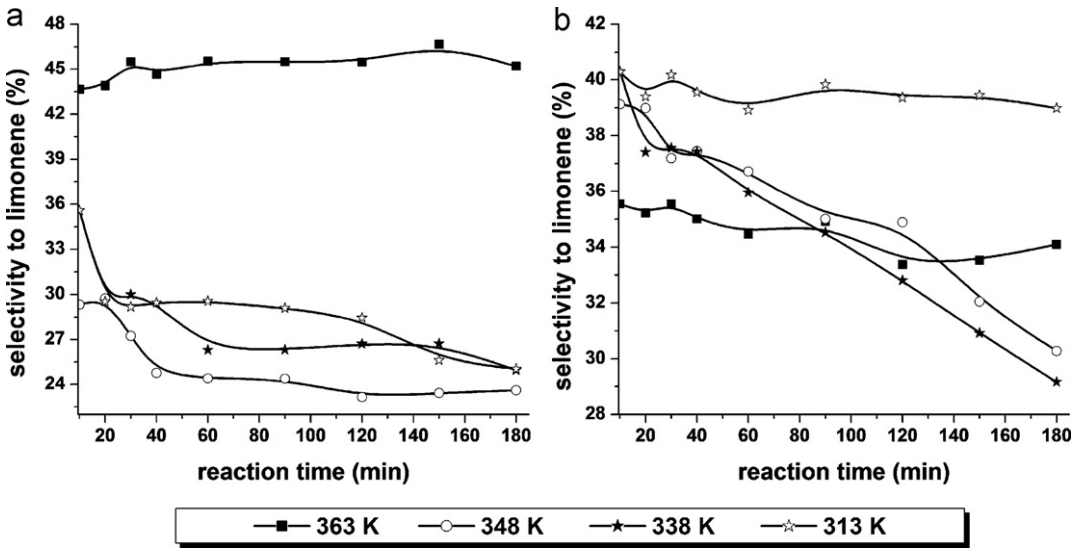
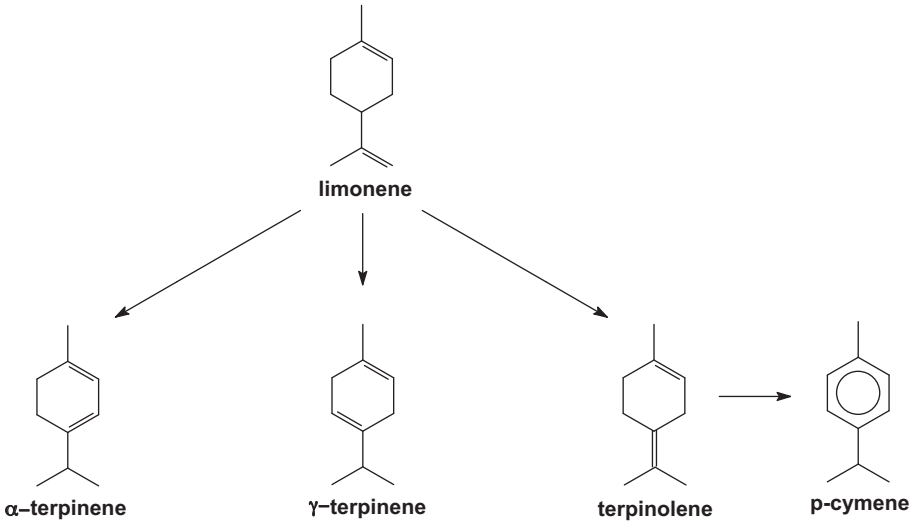


Fig. 8. Selectivity towards limonene vs. the reaction time for the isomerization of α-pinene on (a) H-FER (Z) and (b) H-FER (T) at 313–363 K. The conditions of catalytic tests were as in Fig. 6.



Scheme 2.

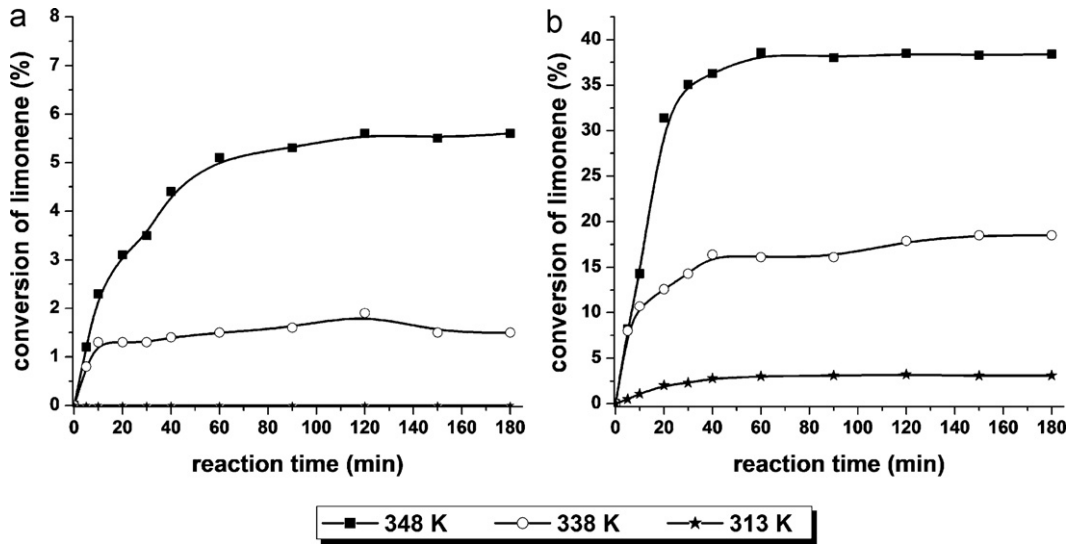


Fig. 9. Conversion of limonene vs. the reaction time for the isomerization reaction on (a) H-FER (Z) and (b) H-FER (T) at 313–348 K. The amount of a catalyst precalcined at 673 K: 0.25 g. Substrate: 5 ml of limonene.

Author's personal copy

the other sample at the same temperatures, although visible, is much less pronounced. These observations confirm that limonene is more reactive than camphene and, therefore, can be probably further transformed, via a carbocation intermediate, into different products of limonene group, such as terpinenes, terpinolenes and p-cymene (cf. Scheme 2).

In order to verify experimentally this assumption, pure limonene was used as a feed and the results of its transformation over the ferrierite catalysts in the temperature range of 313–348 K are depicted in Fig. 9. (At 363 K, the selectivity to limonene is nearly steady during the reaction time studied.) As seen, the conversion of limonene on the two ferrierite catalysts is strikingly different, i.e. significantly higher over the zeolite from Tosoh (38%). At the same temperature conversion over H-FER (Z) hardly exceeds 5%. Limonene is, therefore, easily transformed into different products on H-FER (T). On the other hand, the H-FER (Z) catalyst, exhibiting Brønsted acid sites of the higher strength and containing more faults as well as more extraframework aluminium, tends to produce more oligomeric species during the transformation of α-pinene. The presence of such species inhibits efficiently formation of by-products and directs the isomerization of α-pinene to the main primary products, camphene and limonene.

Due to lower formation of oligomeric products, isomerization of pure limonene proceeds more easily over zeolite H-FER (T) at 348 and 338 K. On this catalyst, limonene undergoes facile transformations to other hydrocarbons of the limonene group, like α- and γ-terpinene, terpinolenes and *p*-cymene (Scheme 1 and Fig. 9). At about 313 K, the isomerization of limonene is essentially stopped (Fig. 9b). Therefore, in the transformation of pure α-pinene, the selectivity to limonene vs. the reaction time remains practically constant at this temperature, while it is decreasing by ca. 10% at 338 and 348 K (Fig. 8b).

4. Conclusions

We have shown that α-pinene can be transformed effectively over the hydrogen forms of ferrierite of different origin. The initial reaction rates of α-pinene are high, and in general exceed those found for other classes of catalysts, heteropolyacids and sulphonated zirconium oxide. The characteristic behaviour of α-pinene conversion vs. the reaction temperature can be related to the formation of oligomeric products and the ability of a catalyst to isomerize further the limonene formed. Formation of oligomeric products is more pronounced on the ferrierite containing Brønsted sites of higher acid strength. The H-FER (T) sample exhibits, at 363 K, a higher selectivity towards camphene and a lower one to limonene than the H-FER (Z) material does. Deposition of the HRTP products, observed for both catalysts at 363 K, prevents efficiently consecutive reactions and, therefore, favours the formation of camphene and limonene from α-pinene. Limonene can be further isomerized over the ferrierite from Tosoh at 348 and 338 K giving terpinenes, terpinolenes and finally *p*-cymene. These consecutive transformations of limonene, one of the two primary products formed over ferrierite catalysts from α-pinene, are essentially not observed for the H-FER (Z) ferrierite sample containing Brønsted sites of higher acid strength. Different characteristics of the acid sites in the zeolite materials under study with the same architecture is thus responsible for their particular catalytic behaviour in the transformations of pure α-pinene and pure limonene.

Acknowledgements

We are grateful to Professor J. Datka and Dr. K. Góra-Marek of the Jagiellonian University, Kraków, for the IR measurements. B.S. is indebted to the Ministry of Science and Higher Education for the NMR 500 MHz spectrometer equipment grant (project No. 75/E-68/S/2008-2). The ferrierite samples were kindly supplied by Tosoh Corporation (Japan) and Zeolyst International (US).

References

[1] C.S. Sell, The Chemistry of Fragrances From Perfumer to Consumer, 2nd ed., The Royal Society of Chemistry, Cambridge, 2006.
[2] C.S. Sell, A Fragrant Introduction to Terpenoid Chemistry, The Royal Society of Chemistry, Cambridge, 2003.
[3] E. Breitmaier, Terpenes, Wiley-VCH, Weinheim, 2006.
[4] V.P. Wystrach, L.H. Barnum, M. Garber, J. Am. Chem. Soc. 79 (1957) 5786–5790.
[5] A. Severino, A. Esculcas, J. Rocha, J. Vital, L.S. Lobo, Appl. Catal. A: Gen. 142 (1996) 255–278.
[6] R.G. Berger, Flavours and Fragrances, Chemistry, Bioprocessing and Sustainability, Springer-Verlag, Heidelberg, 2007.
[7] K. Bauer, D. Garbe, H. Surburg, Common Fragrance and Flavor Materials, 4th ed., Wiley-VCh, Weinheim, 2001.
[8] M. Gscheidmeier, R. Gutmann, J. Wiesmüller, A. Riedel, US Patent 5,559,127 (1997).
[9] M. Gscheidmeier, H. Häberlein, H.H. Häberlein, J.T. Häberlein, M.C. Häberlein, US Patent 5,826,202 (1998).
[10] C.M. Lopez, F.J. Machado, K. Rodriguez, B. Mendez, M. Hasegawa, S. Pekerar, Appl. Catal. A: Gen. 173 (1998) 75–85.
[11] A.I. Allahverdiev, G. Gündüz, D.Y. Murzin, Ind. Eng. Chem. Res. 37 (1998) 2373–2377.
[12] A.I. Allahverdiev, S. Irandoust, D.Y. Murzin, J. Catal. 185 (1999) 352–362.
[13] C. Lopez, F. Machado, K. Rodríguez, D. Arias, B. Méndez, M. Hasegawa, Catal. Lett. 62 (1999) 221–226.
[14] R. Rachwalik, Z. Olejniczak, J. Jiao, J. Huang, M. Hunger, B. Sulikowski, J. Catal. 252 (2007) 161–170.
[15] Ł. Mokrzycki, B. Sulikowski, Z. Olejniczak, Catal. Lett. 127 (2009) 296–303.
[16] B. Gil, Ł. Mokrzycki, B. Sulikowski, Z. Olejniczak, S. Walas, Catal. Today 52 (2010) 24–32.
[17] L. Grzona, N. Comelli, O. Masini, E. Ponzi, M. Ponzi, React. Kinet. Catal. Lett. 71 (2000) 27–32.
[18] M.A. Ecormier, A.F. Lee, K. Wilson, Micropor. Mesopor. Mater. 80 (2005) 301–310.
[19] N.A. Comelli, E.N. Ponzi, M.I. Ponzi, J. Am. Oil Chem. Soc. 82 (2005) 531–535.
[20] D.R. Brown, C.N. Rhodes, Catal. Lett. 45 (1997) 35–40.
[21] C. Breen, R. Watson, J. Madejova, P. Komadel, Z. Klapyta, Langmuir 13 (1997) 6473–6479.
[22] O. Masini, L. Grzona, N. Comelli, E. Ponzi, M. Ponzi, J. Chil. Chem. Soc. 48 (2003) 101–104.
[23] N.A. Comelli, L.M. Grzona, O. Masini, E.N. Ponzi, M.I. Ponzi, J. Chil. Chem. Soc. 49 (2004) 245–250.
[24] A.D. Newman, A.F. Lee, K. Wilson, N.A. Young, Catal. Lett. 102 (2005) 45–50.
[25] D. Freude, M. Hunger, H. Pfeifer, G. Scheler, J. Hoffmann, W. Schmitz, Chem. Phys. Lett. 105 (1984) 427–430.
[26] Y. Jiang, J. Huang, W. Dai, M. Hunger, Solid State Nucl. Magn. Reson. 39 (2011) 116–141.
[27] C. Doremieux-Morin, P. Batamack, J.M. Bregeult, J. Fraissard, Catal. Lett. 9 (1991) 403–409.
[28] J. Datka, M. Kawałek, K. Góra-Marek, Appl. Catal. A: Gen. 243 (2003) 293–299.
[29] B. Gil, G. Košová, J. Čejka, Micropor. Mesopor. Mater. 129 (2010) 256–266.
[30] E.A. Paukstis, E.N. Yurchenko, Usp. Khim. 52 (1983) 426–454.
[31] B.G. Harvey, M.E. Wright, R.L. Quintana, Energy Fuels 24 (2010) 267–273.
[32] J. Datka, B. Gil, J. Węglarski, Micropor. Mesopor. Mater. 21 (1998) 75–79.